Using Acoustic Micro Doppler Sonar to Distinguish between Human and Equine Motion

Dr. Marshall Bradley and Dr. James M. Sabatier
University of Mississippi
National Center for Physical Acoustics
University, MS 38655 USA

marshall.bradley@gmail.com / james.sabatier@us.army.mil

ABSTRACT

The influx of unauthorized immigrants into the United States presents multiple security issues. A need exists for a low-cost, low-false alarm distributable surveillance system that can enhance border security. Sensors such as geophones and microphones can detect the presence of a walking individual but they cannot reliably distinguish between human motion and other natural sources of movement and sound. Along the southern border between the United States and Mexico there are significant amounts of equine wildlife. Presently available sensor modalities cannot reliably distinguish between a walking horse and a walking human. One sensor type that has the capability to distinguish between the motions of human and horse is the acoustic micro Doppler sonar. Doppler sonar grams are known to provide a wealth of information about human gait. Individual body parts have different acoustic cross-sections and velocities resulting in unique Doppler signatures. Similar signatures are measured by Doppler radar systems. This is not surprising since sonar and radar operate at comparable wavelengths. In this paper observed human-gait features in Doppler sonar grams are explained by using the Boulic-Thalmann (BT) model to predict joint angle time histories and the temporal displacements of the body center of mass. In order to facilitate the comparison between human and horse signatures, a new empirical model of horse motion is developed based upon equine joint angle time histories and ground reaction forces. For both the horse and human, body segments are represented as ellipsoids whose parameters are determined from appropriate anthropomorphic data. Temporally dependent velocities at the proximal and distal end of key body segments are determined for humans from the BT model. For horses, the new motion model is used. Doppler sonar grams are computed by mapping velocity-time dependent spectral acoustic-cross sections for the body segments onto time-velocity space, mimicking the Short Time Fourier Transform used in the Doppler sonar processing. The theoretical approach is validated by comparisons to measured micro Doppler sonar grams. For both the human and the horse it is found that the swinging of the legs and motion of the body in response to ground reaction forces produce the dominant returns. The model is then used to identify key differences between the gait of humans and horses that can be exploited by surveillance systems

1.0 INTRODUCTION

Acoustic micro Doppler sonar grams provide a great deal of information about the locomotion of humans and horses. Figure 1 compares a micro Doppler sonar gram of a human walking to horse walking. Both the human and horse are walking towards the sonar at a speed of about 3 mph (1.34 m/s). The sonar is located about 1.5 m above the ground and is transmitting a 40 kHz CW tone that was digitized at 96 kHz. The two grams were formed by taking the short time Fourier transform (STFT) of the digitized signal. The horizontal axis in the figure spans a time range of 18 sec. The vertical axis in the grams is frequency spanning a range corresponding to -8 to 8 m/s in Doppler velocity. There are obvious differences in the grams but there are

many similarities as well. When the horse is close to the sonar, both the motions of the fore and hind legs can be seen. At greater distances motion from only the fore legs are visible, suggesting that the rear leg echoes have been occluded. Previously, an acoustic model based upon the Boulic-Thalmann (BT) human motion model (Boulic 1990) and Fresnel-Kirchoff diffraction theory has been developed and successfully used to describe observed features in micro Doppler sonar grams (Bradley and Sabatier 2011). Predictions from this model have been experimentally verified (Mehmood 2010). In order to distinguish between equine and human motion characteristics, this same modeling approach has been applied to the walking and trot gaits of the horse.

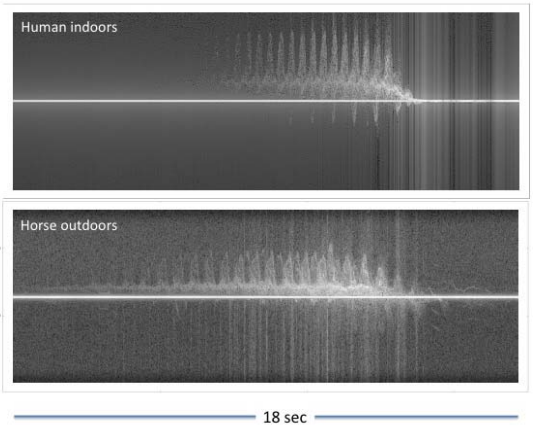

Fig. 1. Human and horse micro Doppler sonar grams.

2.0 TIMING OF THE WALK CYCLE

Figure 2 compares the walking cycle of the human to the horse. Stance phases in which one foot or hoof is on the ground are indicated by dark bars. Swing phases in which legs are being propelled forward are indicated by white bars. During walking, the human always has at least one foot on the ground. Otherwise, the individual would be running. The human walk cycle consists of two steps, one each with the left and right legs. By convention the cycle begins with left heel strike (HS). The order of events in a human walk cycle is as follows: 1) Left heel strike (HS), 2) Right toe off (TO) , 3) Right heel strike, 4) Left toe off, and 1') The left heel strikes the ground for the second time and the walk cycle ends (1=1'). During the time intervals 1-2 and 3-4 the human has two feet on the ground. The length of these intervals is known as the duration of double support. During the time intervals 2-3 and 4-1' the right and left legs are respectively being swung forward.

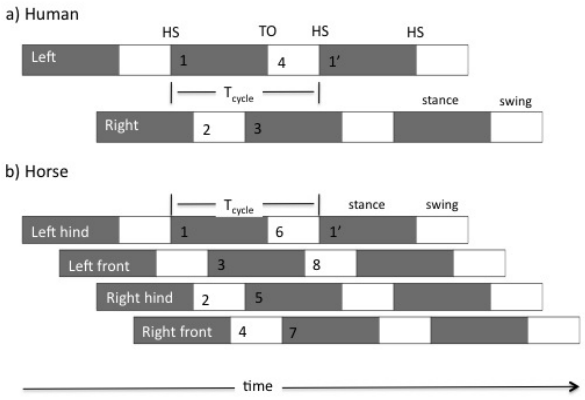

Fig. 2. Human and horse walk cycle timing diagram.

The walking cycle of the horse consists of four steps, one with each leg. As with the human it consists of one complete cycle of limb movements. The timing of foot falls during the horse walk cycle by convention is left hind (LH), left front (LF), right hind (RH) and right front (RF). In a regular walk the four footfalls are equally spaced in time and the time between successive foot falls is one-fourth the cycle time or stride duration (Clayton 2004). The order of events in the walk cycle is as follows: 1) The left hoof strikes the ground and the animal is supported by three legs. 2) The right hind leaves the ground and the animal is supported by two diagonal legs that are close together. 3) The left front hoof strikes the ground and the horse is supported by three legs. 4) The right front hoof leaves the ground and the horse is supported by two legs on the left side. 5) The right hind hoof strikes the ground and the horse is supported by three legs. 6) The left hind hoof leaves the ground. 7) The right front hoof strikes the ground and the horse is supported by three legs. 8) The left front hoof leaves the ground and the horse is supported by two legs. 1') The left hind hoof srikes the ground for the second time and the cycle begins again (1=1'). A careful examination of figure 2a-2b reveals an extremely important characteristic of the walking gait of the horse. It is identical in timing to two people walking out of step. Thus any sensor that relies only on footfall timing could not reliably distinguish between a walking horse and two humans walking out of step.

The time interval T_{cycle} required to complete a walk cycle is an important parameter in characterizing human and horse walking. Relative time over the course of a walk cycle is $\tau = t / T_{cycle}$ and during the course of one complete walk cycle, τ will vary between 0 and 1 for both the horse and the human. Inman (1981) presents a relationship between a person's stride length, body height and step frequency. Stride length is the distance covered in two steps, one with the right foot and one with the left foot. Stride length is twice the step length. A person's average velocity of walking is the step length times the step frequency. Inman's relationship is

$$\frac{\text{stride length/body height}}{\text{step frequency/min}} = 0.008 .$$

Inman states that this equation is useful only as a reference for men. Women will typically have a shorter stride length and the slope of the line relating step frequency/min to stride length/body height will be less steep with a nonzero vertical axis intercept.

If stride length is denoted by *SL* and step length by *sl*, both measured in meters, then $SL = 2sl$. If *SF* denotes

step frequency measured in steps/min and *sf* denotes step frequency measured in cycles/sec, then $SF = 60sf$. If *v* denotes the average walking velocity, then $v = sl \cdot sf$. With these definitions, Inman's law becomes $(sl / bh) / (60sf) = 0.008$. Using the relationship $v = sl \cdot sf$ leads to an equivalent form of Inman's law $T_{cycle}(v, bh) = 0.980(bh / v)^{1/2}$,

where $T_{cycle}(v, bh)$ is the duration of the walk cycle (cycle time) as a function of the walking velocity *v* and body height *bh*. Figure 3 compares Inman's law for the human-walk cycle time to the horse walk cycle time. The curve for the horse is based upon empirical data presented in Back (2001). For a given speed of advance, the horse walk cycle time is slightly smaller that the human walk cycle time.

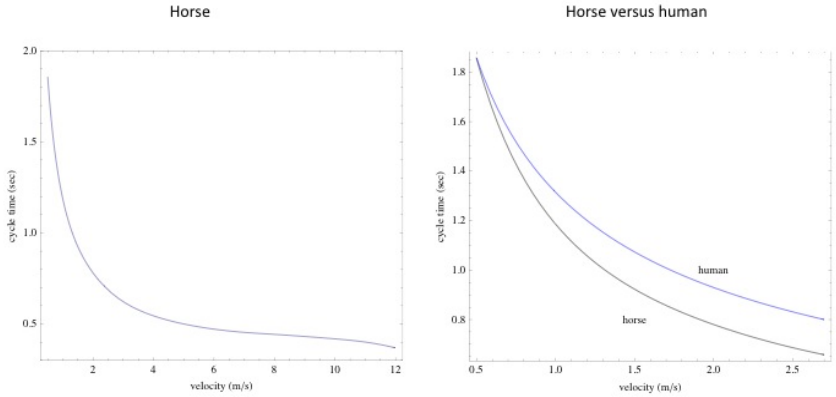

Fig. 3. Comparison of walk cycle times for the human and the horse as a function of walking velocity.

3.0 SEGMENTED LINK MOTION MODEL

In this paper the observed features in equine Doppler sonar grams are explained using a technique previously applied to human motion (Bradley, 2010). The human body was represented as a segmented link system. The Boulic-Thalmann (1990) model was used to predict joint angle time histories and the temporal displacements of the body center of mass. The velocity at the proximal and distal end of each key body segment as a function of time was determined from the Boulic-Thalmann (BT) joint rotations and body translations using simple rigid body physics as described in Bradley (2009). Scattering was assumed to occur from seven types of body segments/parts: the foot, lower leg, thigh, trunk, head-neck, upper arm and lower arm-hand. For the purposes of scattering, the body segments were modeled as rigid ellipsoids. The dimensions of these ellipsoids were estimated from the segment length, mass and density using anthropomorphic data from Winter (2009). At-rest acoustic scattering cross-sections for the segments were determined using Fresnel-Kirchhoff diffraction theory. Velocity and time dependent spectral acoustic-cross sections were obtained by exploiting the fact that the velocity at points on a rotating-translating rigid body must continuously vary across its length. Doppler sonar grams were computed by mapping the time dependent spectral acoustic-cross sections of the various body segments onto time-velocity space. This mapping was implemented in a way that represented the Short Time Fourier Transform (STFT) used in the processing of Doppler sonar data.

The segmented link model that is used to represent the major components of equine motion is shown in the left side of figure 4 and is adapted from Clayton (2004). Equine motion is considerably more complicated than human motion due to the presence of 4 legs and larger number of rotating joints. Front leg sagital plane motion of the horse is determined by rotation at six joints. From proximal to distal they are the scapula, shoulder, elbow, carpus, fore fetlock and fore coffin. The carpus joint corresponds to the human wrist and the fore fetlock and coffin joints correspond to human finger joints. For the human, sagital plane leg motion is primarily determined by rotation about only the hip, knee and ankle. Hind leg sagital plane motion of the horse is controlled by rotation at five joints. From proximal to distal they are the hip, stifle, tarsus, hind fetlock and hind coffin. The pelvis is represented as a joint in the segmented link model but there is no rotation. The stifle and tarsus respectively correspond to the human knee and ankle. The hind fetlock and coffin joints correspond to human toe joints. The horse can be thought of as walking and trotting on finger and toe tips.

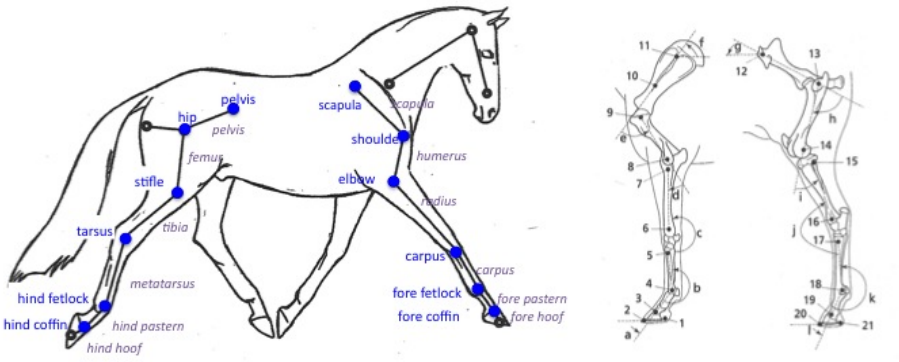

Fig. 4. Segmented link equine motion model.

The segments in the equine segmented link model represent the bones that extend between the joints. For the foreleg from proximal to distal they are the scapula, humerus, radius, fore pastern and fore hoof. For the hind limb from proximal to distal they are the pelvis, femur, tibia, metatarsus, hind pastern and hind hoof. Additionally, the horse flexes and extends its spine during the course of the gait cycle. The hind and rear quarters as well as the head move in a complicated fashion. The joint angle convention used to represent joint rotation is shown in the right side of figure 4 and is based upon a convention from Back (2001). The scapula angle *f* and the pelvic angle *g* shown in the right side of figure 4 are measured with respect to the horizontal. All other joint angles are measured with respect to the joint above. Segment lengths, masses and densities used in the model are based upon Buchner (1997) and are shown in tables 1 and 2. Buchner's data were based upon measurements made on horses that had been destroyed because of illness. Buchner's segment length data (columns labeled *L1* in tables 1 and 2) did not produce a visually correct representation of the horse. Because of this, segment lengths in the model are based upon measurements of the distances between joints in the figure shown in the right side of figure 4. These segment lengths were scaled to the height of the horse and found to produce a much more visually correct result. They are shown in the columns labeled *L2* in tables 1 and 2.

Angle	Joint	Segment	L1(m)	L2(m)	Θ(deg)	M(kg)	ρ(gm/cm³)
f	scapula	scapula	0.274	0.354	50.4	11.5	1.043
e	shoulder	humerus	0.25	0.313	65.6	8.6	1.048
d	elbow	radius	0.434	0.407	-26.5	6.7	1.12
c	carpus	carpus	0.287	0.309	0.551	1.59	1.29
b	fore fetlock	fore pastern	0.135	0.091	-43.3	0.73	1.25
a	fore coffin	fore hoof	0.099	0.108	3.20	1.08	1.181

Table 1. Horse foreleg anthropomorphic data.

Angle	Joint	Segment	L1(m)	L2(m)	Θ(deg)	M(kg)	ρ
g	pelvis	pelvis	0.345	0.319	159.1	nm	nm
h	hip	femur	0.360	0.405	-74.7	18.6	1.047
i	stifle	tibia	0.434	0.411	36.5	8.3	1.09
j	tarsus	metatarsus	0.353	0.350	-18.0	2.84	1.284
k	hind fetlock	hind pastern	0.141	0.105	-39.5	0.89	1.23
l	hind coffin	hind hoof	0.101	0.105	0.00	0.99	1.179

Table 2. Horse hindleg anthropomorphic data.

Joint angle rotation data as a function of time during the course of the gait cycle is taken from Back (2001). Back presents joint rotation measurements for the fore and hind limb joints for a variety of gaits including the walk and the trot. These data have been digitized to support numerical prediction. An example of joint rotation for the carpus joint is shown in figure 5. The shapes of the curves for the walk and the trot are quite similar but when the horse is at the walk, rapid joint motion for the carpus is delayed to a much later time period in the gait cycle. The effect of the rotation of all the hind leg and front leg joints is illustrated in figure 6. These diagrams show the instantaneous position of the hind and front leg segments over the course of a complete walk cycle. Direction of motion of the animal is denoted by the arrow. Distal segments move more than proximal segments due to the combined effect of rotation through more joint angles. The most distal segments, the hooves, clearly move the most and therefore will have the highest velocities when detected on a micro Doppler sonar gram.

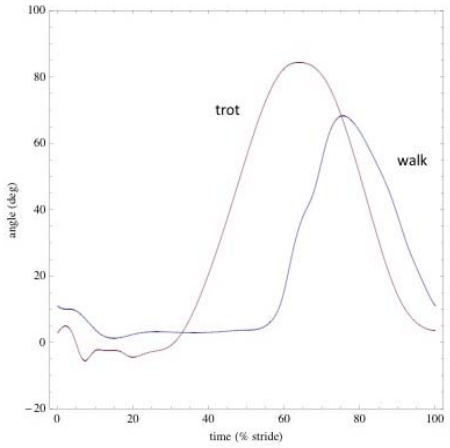

Fig. 5. Rotation of the carpus joint.

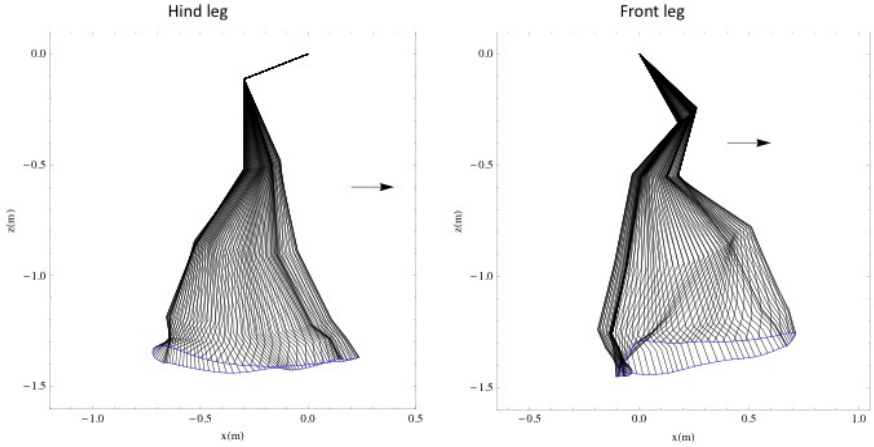

Fig 6. Stick diagrams for the horse at the walk.

4.0 CENTER OF MASS MOTION

The segmented length motion model described in the previous section provides a realistic description of the motions of the hind and fore legs of the horse. However, there are other components of the motion of the horse that are important from the standpoint of micro Doppler sonar. For the human it was previously found that the motion of the torso produces a large sonar echo that is directly related to the bipedal gait cycle. During the course of the walk cycle, the human takes two steps thereby speeding up and slowing down twice. This causes the torso to oscillate at a frequency that is twice the gait frequency. Because of the larger size of the human torso in comparison to the legs and arms, the torso echo velocity, although small in velocity change, is large in amplitude and is easily detected on micro Doppler sonar grams. Torso velocity and displacement for the human can be determined from ground reaction forces and their effect on the motion of

the center of mass (Tsutsuguchi-2000). In this section the approach of Tsutsuguchi is applied to the problem of estimating the torso motion of the horse.

Let $x(t)$, $y(t)$ and $z(t)$ denote the position of the center of mass (COM) of a moving individual (human or horse) at time t in the progressive, lateral and vertical directions. Newton's second law leads to the following set of equations for the motion of the center of mass:

$$m\ddot{x} = F(t), \quad m\ddot{y} = G(t), \quad m\ddot{z} = CH(t) - mg,$$

where $F(t)$, $G(t)$ and $H(t)$ are respectively the ground reaction forces in the progressive, lateral and vertical directions, m is the mass of the body and g is the acceleration due to gravity. The constant C in the third equation is a normalization constant chosen to insure that that the vertical ground reaction force $H(t)$ properly balances the effects of gravity. These three equations can be solved by direct integration. Unknown coefficients that result from these integrations can be found by requiring the solutions for velocity and position to be periodic in the time T_{cycle} required to complete one full gait cycle. This time is two steps for a human and four steps for a walking horse. The solutions to the differential equations for steady state walking are

$$x(t) = x(0) - \frac{F_2(T_{cycle})}{T_{cycle}} t + \frac{1}{m} F_2(t),$$

$$y(t) = y(0) - \frac{G_2(T_{cycle})}{T_{cycle}} t + \frac{1}{m} G_2(t),$$

$$z(t) = z(0) + g\left[\tfrac{1}{2} T_{cycle} - \frac{H_2(T_{cycle})}{H_1(T_{cycle})} \right] t + \frac{g T_{cycle}}{H_1(T_{cycle})} H_2(t) - \tfrac{1}{2} g t^2,$$

where the subscripts on force functions indicate the number of integrations with respect to time, e.g.

$$F_1(t) = \int_0^t F(t_1) dt_1, \quad F_2(t) = \int_0^t F_1(t_2) dt_2.$$

These solutions exploit the fact that in steady state walking, the progressive and lateral ground reaction forces have first integrals that are zero when evaluated at the cycle time T_{cycle}. The unknown initial positions $x(0)$, $y(0)$ and $z(0)$ in the solutions are found by requiring the average position during the course of a walk cycle to be zero.

Tsutsuguchi (2000) presents an analytical model of ground reaction forces in human walking. The progressive, lateral and vertical ground reaction forces for a single foot are

$$F_f(t) = s_x \sum_{k=1}^{3} a_{x,k} \sin\left(\tfrac{2\pi k}{T_{\text{stance}}} t\right) \quad G_f(t) = s_y \sum_{k=1}^{3} a_{y,k} \sin\left(\tfrac{\pi k}{T_{\text{stance}}} t\right) \quad H_f(t) = s_z \sum_{k=1}^{3} a_{z,k} \sin\left(\tfrac{\pi k}{T_{\text{stance}}} t\right)$$

where s_x, s_y and s_z are scale factors that depend on the speed of walking and T_{stance} is the duration of stance, i.e. the time interval when one foot is on the ground. For an individual walking at 3 mph the scale coefficients are approximately unity. If T denotes the duration of a single step, then $T_{\text{stance}}=T+T_{\text{ds}}$ where T_{ds} is the duration of double support. For human walking it is approximately true that $T_{\text{ds}}=0.25T$ and that $T_{\text{stance}}=0.6125T_{\text{cycle}}$. For walking on level ground, Tsutsuguchi (2000) defines the Fourier coefficients describing progressive motion to be $a_{x,k}=-0.14286/2^{k-1}$ for $k=1, 2, 3$. For the lateral and vertical components of motion the coefficients are $(a_{y,1},a_{y,2},a_{y,3})=(0.07,-0.03,-0.03)$ and $(a_{z,1},a_{z,2},a_{z,3})=(1.3,0.1,0.4)$.

Foot and hoof ground reaction forces for a walking human and horse are compared in figure 7. The foot ground reaction forces have been estimated using the Tsutsuguchi model. Hoof ground reaction forces were taken from Back (2001). The forces are scaled by body weight. Since the horse always has at least two feet

on the ground during walking, the peak ground reaction forces are about half those for the human. Fore leg ground reaction forces are higher for the horse in comparison to the hind leg ground reaction forces. The upper portion of figure 8 compares total walk cycle ground reaction forces for the human to the horse. COM velocity solutions for the human and horse are compared in the lower portion of figure 8. The progressive component of velocity for the horse clearly shows the effects of four steps in a walk cycle. Figure 9 compares the COM displacement solution for the human to the BT model for displacement. The agreement is quite good. COM predicted velocities for the human and horse are compared to data in figure 10.

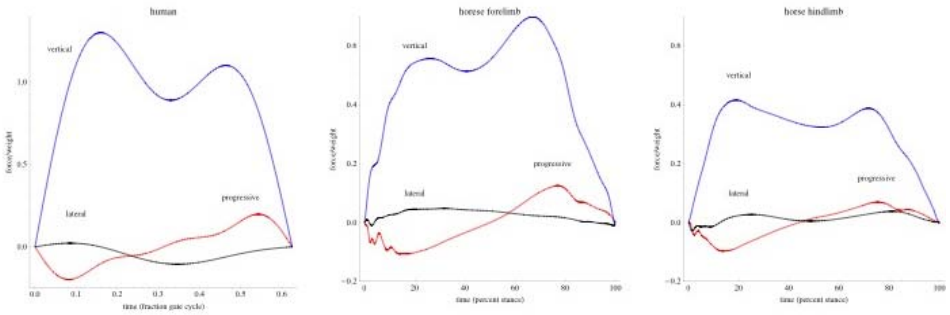

Fig 7. Foot and hoof ground reaction forces.

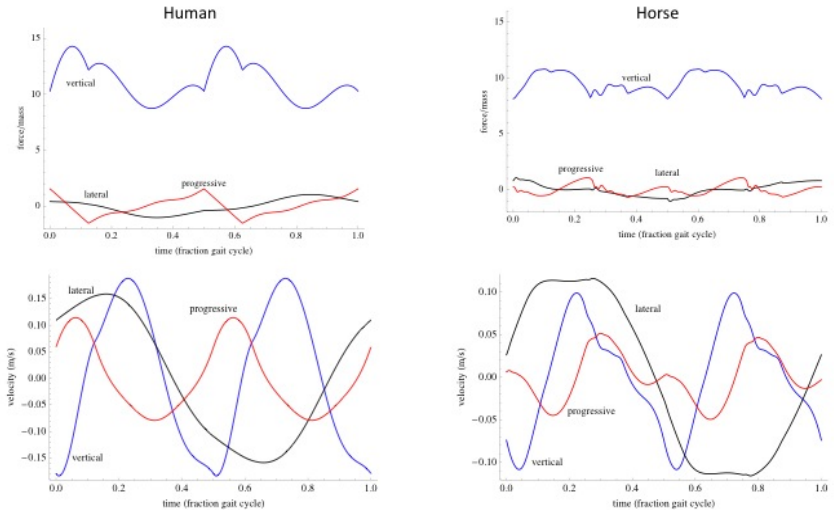

Fig. 8. Ground reaction forces and center of mass velocity for the human and horse.

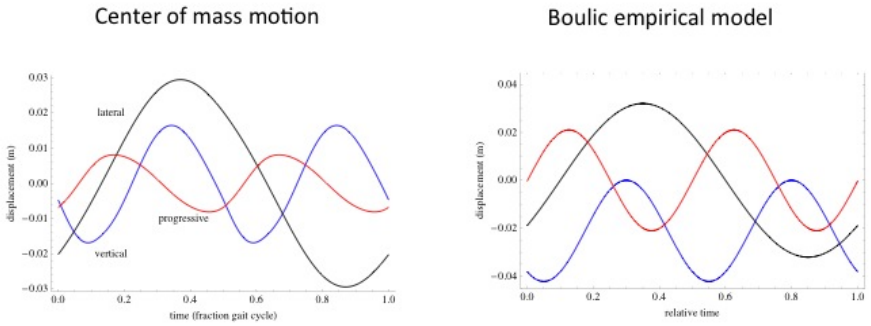

Fig. 9. Center of mass displacement for the human compared to Boulic-Thalmann model.

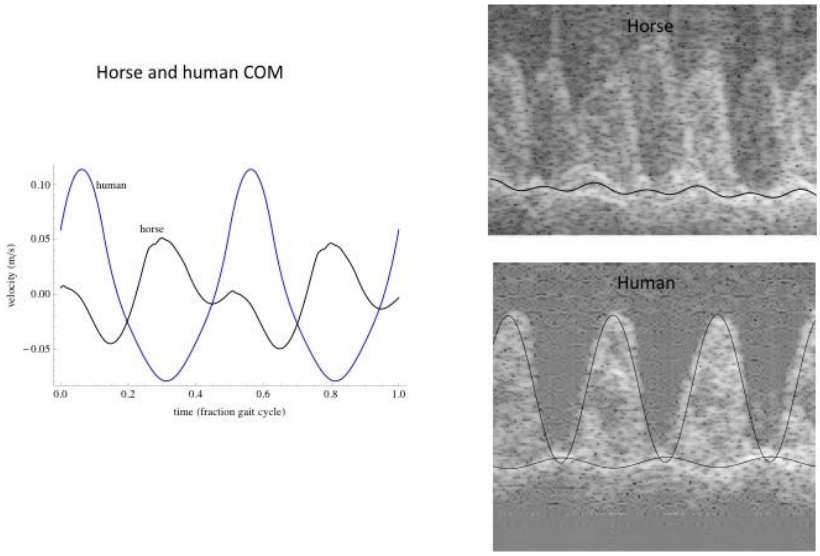

Fig. 10. Measured and modeled torso velocity comparison.

5.0 ANALYSIS AND DATA COMPARISONS

The contributions from the right hind and front legs of a walking horse to a micro Doppler sonar gram is shown in figure 11. The dynamic range in the plots is 60 dB. The time epoch for the model prediction covers approximately two cycles of walking. The walk cycle begins with left rear hoof strike of the horse (not shown in the figure). This is immediately followed by the right hind leg swinging forward. Next right heel strike occurs. Then the horse swings the right leg to the rear. During this rearward leg swing a peak negative velocity for the right hoof of about – 2m/s is achieved. The right hand side of figure 11 shows the corresponding prediction for the right front leg. The velocity structure in the gram for the front leg is very different than for the hind leg. The front leg reaches higher peak velocities in shorter amounts of time. Figure

12 compares predicted micro Doppler sonar grams for a human walking to a horse walking. In both figures 11 and 12, the walking speed is 1.34 m/s. The horse front leg reaches higher velocities than the human leg and both the front legs and hind legs of the horse have higher negative velocities than do the legs of the human. Figure 13 compares a predicted micro Doppler sonar gram to a measurement during a time period when both the front and hind legs of the horse can be seen by the sonar. The rapid forward swing of the horse leg can be seen in the measurement and the model.

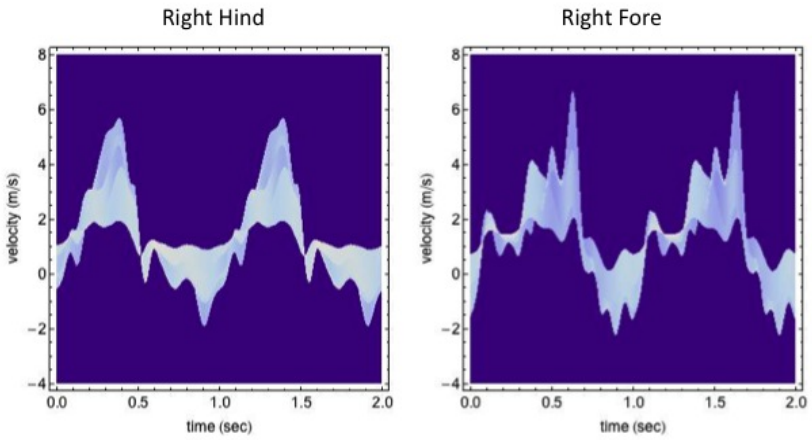

Fig. 11. Contributions of hind and front legs to horse micro Doppler signature.

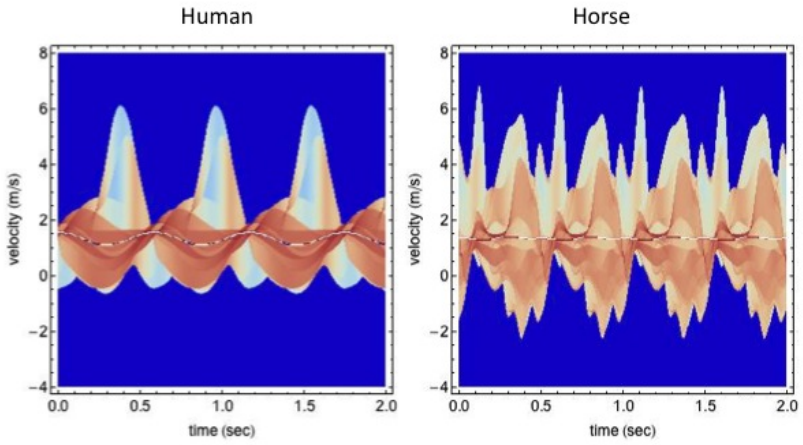

Fig. 12. Predicted micro Doppler sonar grams for human and horse walking.

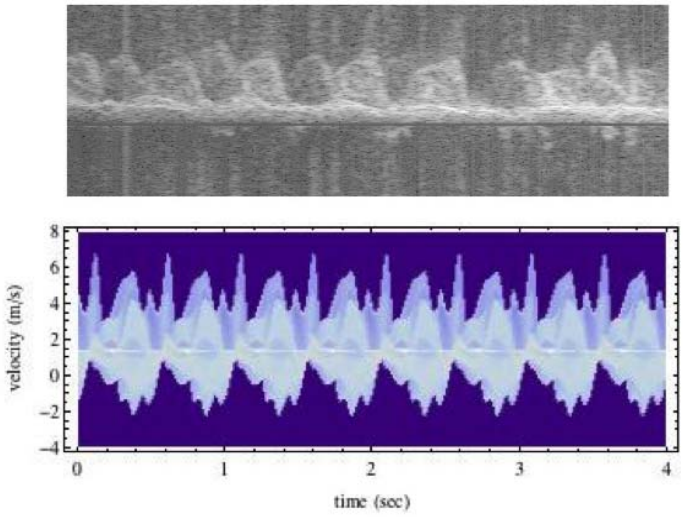

Fig. 13. Measured and predicted horse micro Doppler sonar grams.

6.0 REFERENCES

Back, Willem and Clayton, Hilary. (**2001**). *Equine Locomotion* (W. B. Saunders, New York).

Boulic, R., Thalmann, N. and Thalmann, D. (**1990**). "A Global Human Walking Model with Real-Time Kinematic Personification", Visual Computer 6, pp. 344 - 358.

Bradley, M. (**2009**). "A Mathematical Implementation of a Global Human Walking Model with Real-Time Kinematic Personification by Boulic, Thalmann and Thalmann", Human Light Vehicle and Tunnel Detection Workshop, June 16-17, 2009.

Bradley, Marshall and Sabatier, James (**2010**). "Applications of Fresnel-Kirchhoff diffraction theory in the analysis of human-motion Doppler sonar grams", JASA, Vol 128, Issue 5, pp. EL248-EL253.

Buchner, H. H. F., Savelberg, H. H. C. M., Schamhardt, H. C. and Barnveld, A. (**1997**). "Inertial properties of Dutch warmblooded horses", J. Biomechanics", Vol. 30, No. 6, pp. 653-658.

Clayton, Hillary M. (**2004**). *The Dynamic Horse* (Sport Horse Publications, Mason MI).

Inman, V., Ralston, H. and Todd, F. (**1981**). *Human Walking* (Williams & Wilkins, Baltimore/London).

Mehmood, A., Sabatier, J., Bradley, M. and Ekimov, A. (**2010**). "Extraction of the velocity of walking human's body segments using ultrasonic Doppler", JASA, Vol 128, Issue 5, pp. EL316-EL322.

Winter, D. (**2009**). *Biomechanics and Motor Control of Human Movement* (Wiley, Hoboken NJ).